



Simulation of sputtering induced by high energy gold clusters [☆]

M.H. Shapiro ^{a,b,*}, T.A. Tombrello ^b

^a Department of Physics, California State University, P.O. Box 6866, Fullerton, CA 92834-6686, USA

^b Division of Physics, Mathematics and Astronomy, California Institute of Technology, Pasadena, CA 91125, USA

Received 6 October 1998; received in revised form 19 January 1999

Abstract

Recently Andersen et al. reported exceptionally large nonlinear sputtering yields following the bombardment of gold targets with small, high energy gold clusters (H.H. Andersen, A. Brunelle, S. Della-Negra, J. Depauw, Y. LeBeyec, Phys. Rev. Lett. 80 (1998) 5433). Nonlinearities up to $\sim 1000\%$ were observed for Au₅ clusters with a total energy of 800 keV. We have carried out molecular dynamics simulations on a massively parallel computer to model the Au_n → Au system. The results suggest that both collisional and thermal spike mechanisms contribute to the large nonlinear yields observed by Andersen et al. Our simulations also indicate that sputtering statistics are very important at high cluster bombarding energies. A substantial fraction of the simulated impacts produce no sputtered atoms, while individual sputtering events producing very large numbers of sputtered atoms contribute significantly to the total sputtering yield at high energy. © 1999 Elsevier Science B.V. All rights reserved.

1. Introduction

Andersen et al. [1] recently investigated sputtering from thick gold targets induced by fast gold atoms and small gold clusters (up to Au₅). They obtained sputtering yields at bombarding energies ranging from ~ 20 keV/atom to ~ 2 MeV/atom for monomers, dimers, and trimers; and, from ~ 20 keV/atom up to 500 keV/atom for tetramers and pentamers. These yield data exhibited two striking

features. First, very large nonlinearities were observed in the sputtering yields induced by the small gold clusters. For example, at 150 keV/atom bombarding energy the yield (Y) was ~ 3000 for Au₅ clusters, but only ~ 55 for monomers with the same velocity. Second, the maximum in the sputtering yield occurred at the same *total* energy for all clusters. Indeed, if Y/n^2 is plotted against total cluster energy for their data remarkably similar curves are seen for $n=2$ through $n=5$. (However, the yield curve for monomers is significantly broader in energy, and the collisional energy loss is broader still.)

The thick gold targets used to obtain the results in Ref. [1] were deposited on the quartz crystal of a crystal-oscillator microbalance. The experimental sputtering yields were obtained by measuring the

[☆] Supported in part by the National Science Foundation (grants DMR-9312468 and DMR-9712538 at Cal State Fullerton and DMR-9730893 at Caltech).

* Corresponding author. Tel.: +1-714-278-3884; fax: +1-714-278-5810; e-mail: mshapiro@fullerton.edu

amount of mass removed from the quartz crystal. Thus, the reported yields included both sputtered neutrals and charged ions integrated over all energies and sputtering angles.

The dependence of the yield on total cluster energy was attributed to the nonlinearity in the sputtering process. However, attempts to account for the observed nonlinear yields as a sum of the linear cascade yield [2,3] and thermal spike surface evaporation [4] as Sigmund and Claussen had done at lower energies proved unsuccessful. It was not possible to find a single value for the initial radius ρ_0 of the spike that would work for all values of n , over the energy range for which the data were obtained. In addition, Andersen et al. were not able to provide an explanation for the dependence of the yield on n^2 .

The present work is an attempt to understand the reasons for the large nonlinear yields seen in the experiments of Ref. [1]. We have carried out molecular-dynamics (MD) simulations on a massively parallel computer for Au₁, Au₂, and Au₃ projectiles impacting gold targets at energies up to 1000 eV/atom. Owing to computational limitations it was necessary to carry out these simulations with target crystallites containing about 12,000 or fewer atoms. These targets had dimensions large enough in the directions transverse to the incident beam to contain the lateral spread of the collision cascades for most impacts. However, they were too thin to produce the yields observed experimentally. To compensate, the MD code was modified to permit a fraction of the energy transmitted through the rear surface of the target to be reflected back into the target. With this modification it was possible to adjust the yields for monomer bombardment to be close to the experimentally observed values.

The modified code was used to investigate atom ejection for up to 3000 fs following impact by monomers, dimers, and trimers. Our results suggest that both collisional and thermal spike mechanisms contribute to the large nonlinear yields seen in the experiments of Andersen et al. In addition, our simulations suggest that individual sputtering events with very large yields (“mega-events” [5]) contribute significantly to the total sputtering yields at these high bombarding energies.

2. Simulation model

The simulations reported in this paper were carried out with a version of the SPUT2 MD code [6] that was modified for use on a 512-node Intel Paragon parallel computer (Trex) at Caltech. The SPUT2 single processor code was modified to include a manager routine that operated in one node, and a worker routine that operated in each of the other nodes. The manager routine had two primary tasks. The first task was to create a list of impact locations for incident projectiles that scanned the primary impact zone of the target, and to send these starting locations to the worker nodes. The second task was to organize the output from each of the worker nodes into a small number of files for later analysis.

To perform its first task the manager program created a list of impact locations that scanned the primary impact region of the target. For dimers and trimers the orientation of the projectile relative to the target surface was chosen randomly for each impact. The list of impact locations was ordered by impact parameter. Locations with the smallest impact parameters, which were expected to take the most time to finish, were sent to the worker nodes first. This helped to optimize the load on the Paragon.

When a worker node had completed the integration of an impact, it would send a message to the manager node. The manager program would then send a new impact location to the open node. This process continued until all impacts had been computed or the 12-h block of batch processing time on Trex ran out. The manager node then would combine the information for all completed impacts into two files. One file contained information about the starting locations and exit velocity components for atoms that had sputtered. The other file contained information about the time of sputtering for ejected atoms.

The nodes that were still processing impacts when time ran out, if any, wrote individual files that contained information that could be used to continue the calculation when the next block of processing time became available. The time needed to compute an individual impact varied widely depending on the impact parameter, the

yield for the impact, and the number of target atoms being used for a particular simulation run. Impacts that produced no or little sputtering would finish in an hour or two, while impacts that produced very large sputtering yields would require more than 48 h of computer time to complete.

The worker node program used basically the same integration scheme that was used in the SPUT2 code. This code uses two-body potentials to represent the interactions between atoms. While this is not as realistic as using many-body potentials such as those provided by the embedded-atom method (EAM potentials), the differences between simulations with two-body and EAM potentials are expected to be small [7]. However, the savings in computing time for simulations with two-body potentials vs. EAM potentials is substantial. The two-body Au–Au potentials used in this study included a repulsive core modeled with a Molière potential that was connected to an attractive Morse well with a cubic spline. The parameters for this potential function have been published previously [8].

The SPUT2 MD code incorporates features that enhance computational efficiency. These include a self-adjusting time step [9], neighbor-list logic [6], and a “moving atom” list [6]. For these calculations with large targets (>10,000 atoms), the neighbor-list logic was modified to enhance further the speed of the code. In this modified neighbor-list algorithm, atoms are placed on the neighbor list only if they are (1) moving, or (2) within the force cutoff distance of a moving atom, or (3) within the force cutoff range of atoms placed on the list because they satisfied criterion (2). With this change to the neighbor-list algorithm, the size of the list grows only in proportion to the size of the developing collision cascade. For large targets the savings in computer time during the early stages of the cascade are considerable.

In all versions of the code used in these simulations, electronic energy losses were accounted for with a viscous drag model, i.e. $dE/dx = -Kv = -NS_e$, where N is the average electron density in the target and S_e is the electronic stopping power [10]. (As we have noted elsewhere [11], this approach is valid for collisions with valence elec-

trons. However, it does not account properly for hard collisions, which lead to core-excitation.) The viscous loss model was implemented efficiently in our MD code by multiplying each projectile atom velocity vector component by $(1 - K\Delta t/m)$, where m is the mass of the atom, at each time step.

A correction also was included to account for the recoils of projectile atoms from collisions with the “electron gas” (straggling). We took advantage of the fact that the momentum change of a projectile atom in a projectile-electron collision is at almost right angles to the direction of the projectile’s motion [12] and that the momentum transfer to the projectile is very small, $\sim v_p(2m_e K\Delta t)^{1/2}$. Thus, at each time step, for each of the projectile atoms the program randomly chooses a direction in the plane perpendicular to the projectile atom’s motion and adds a velocity in this direction of (v_p/m_p) . This correction is an order of magnitude smaller than the viscous drag correction.

It was not possible to use the instantaneous energy loss algorithm used in previous MD simulations [11] to account for the inelastic effects of core-excitation owing to the high energy of the projectile atoms in these simulations. However, a “bond-weakening” algorithm was included in some of our simulation runs to obtain a crude estimate of the effects of core-excitation on sputtering yields. This algorithm was based on the assumption that the fast projectile atoms were core-excited, and that this would change the electronic environment in the vicinity of these projectile atoms sufficiently to weaken or eliminate the attractive part of the Au–Au force between atoms in the vicinity of the fast moving projectile atoms. The range of the effect was assumed to be approximately 1.5 nm for a 1 MeV projectile atom, and was assumed to scale with the velocity of the projectile atom. The attractive part of the Au–Au force was turned off for any target atom that was within this range of a projectile atom for that particular time step in the integration. Sputtering yields were higher for simulations that included bond-weakening, but the increase typically was less than 8%, and the effect on nonlinearity was negligible.

The targets used in these simulations had dimensions of approximately $9.8 \text{ nm} \times 9.8 \text{ nm}$ in the directions perpendicular to the incident beam. In the beam direction targets were from six to ten atomic layers thick, depending on the simulation. The nine-layer fcc(111) targets that were used for many simulation runs contained a total of 12,363 atoms. These dimensions were large enough to contain the lateral spread of most collision cascades, but the yields obtained for monomer impacts with the open boundary conditions used in the simulations were typically one-third to one-half of the yields observed experimentally. They also were significantly lower than the yields computed with the TRIM program for thick targets. This was attributed to the fact that at these high bombarding energies a very large fraction of the momentum in the early stages of the collision cascade was being transported through the back surface of the simulation targets. In a thick target some of this lost momentum would be reflected back towards the target surface by collisions deeper in the target. Although atoms moving towards the surface from deep within a thick target seldom sputter, the momentum that they carry towards the surface increases the yield of atoms that sputter from the first several atomic layers of the target.

To compensate for this effect a reflection algorithm was included in some of our simulations. A fraction of the incident ions and target atoms reaching the back surface of the target would have their velocity component along the beam direction reversed to simulate momentum coming back into the surface region from deeper in the target. The amount of reflection could be adjusted separately for incident ions and target atoms. To quench the effect only a single bounce from the back surface was permitted for any projectile. If any reflected particle reached the back surface a second time, it was permitted to continue out of the target. With this reflection algorithm in operation the experimentally observed monomer sputtering yields could be matched reasonably well by reflecting from 10% to 15% of the incident ions and target atoms from the back surface of nine-layer fcc(111) targets.

3. Simulation results

3.1. Preliminary simulations

Our initial simulations were carried out with six-layer fcc(100) and fcc(111) targets, and with amorphous targets that were equivalent in thickness to six and nine-layer fcc(100) targets. These simulations did not include reflections from the back surface of the target or bond weakening. The integration of an impact for these runs was terminated when no particle within the target volume had sufficient energy to sputter, or when a cutoff time of 1000 fs was reached. This was sufficient to provide information about the ballistic phase of the collision cascades, but not sufficient to provide information about the thermal spike phase. A total of 800 impacts were computed for monomers, dimers, and trimers normally incident on the targets at 100, 300, 650 and 1000 eV/atom.

Normalized sputtering yields computed with the six-layer fcc(111) targets are shown in Fig. 1. Similar results were obtained with six-layer fcc(100) and amorphous targets. At the lowest incident energy (100 eV/atom), the computed monomer yields ranged from about 20% to 40% of the experimentally observed values. In contrast to the experimental results, the monomer yields

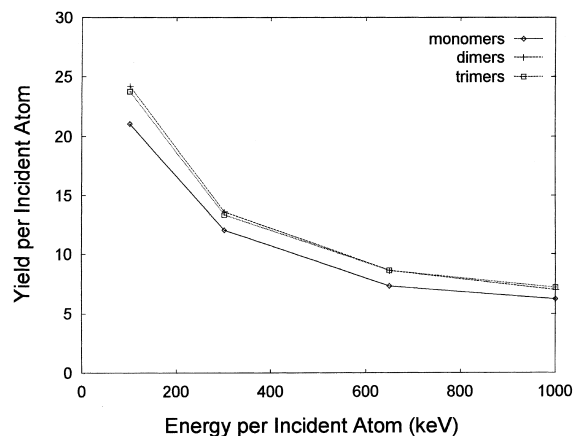


Fig. 1. Normalized sputtering yields computed with six-layer fcc(111) targets and a 1000 fs cutoff time for monomer, dimer and trimer projectiles. Similar results were obtained with six-layer fcc(100) and six-layer amorphous targets.

decrease with increasing incident energy. The computed dimer and trimer yields clearly are nonlinear, but the effect is small compared to the experimentally observed data. Increasing the target thickness from six layers to nine produces a roughly proportional increase in yield. However, the monomer yields still decrease as the incident energy increases, which is an indication that these simulation targets were much too thin and the cutoff time too short to model adequately the Au → Au system at these energies.

Binary collision approximation simulations with the TRIM program were run with target thickness values of 5.0 and 10.0 nm to obtain estimates of the thickness values that would be needed to duplicate the experimentally observed yields. The results suggested that for incident energies up to about 100 eV a target thickness of about 5 nm (~25 atomic layers) would be needed, and for energies above that the targets would need to be at least 10 nm thick (~50 atomic layers) to obtain yields approaching the experimental values. Although the individual nodes of the Paragon could have handled targets of this size, the time needed to complete a statistically significant number of impacts would have been unreasonable.

Instead, additional MD simulations were done with nine-layer fcc(1 1 1) targets using a cutoff time of 3000 fs to permit investigation of the thermal spike regime; and, the reflection algorithm described in Section 2 was used to model the effects of thicker targets. Simulations were done for incident energies of 100 and 200 keV/atom for monomers, dimers, and trimers. Reflection parameters of 0.1 were used for both the incident projectiles and target atoms for the 100 keV/atom

simulations. The “bond weakening” algorithm described in Section 2 was used for the first set of simulations at this energy. In addition, the monomer simulation was repeated with the bond-weakening algorithm turned off. The calculated monomer yields were 70 with bond weakening and 65 without. These values are comparable to the experimentally observed monomer yield at this energy. More detailed yield results are presented in Section 3.3.

3.2. Sputtering statistics

The yield of sputtered atoms varies greatly from impact to impact at the bombarding energies used in these simulations. Relatively large numbers of monomer and dimer impacts (up to 40% of monomer impacts and up to 31% of dimer impacts) were found to yield no sputtered atoms (cf. Table 1), even though the fcc(1 1 1) target orientation used in these simulations is relatively opaque. For trimers the number of impacts that yielded no sputtered atoms was smaller but still ranged from 9% to 22%, depending on the bombarding energy and reflection parameters that were used.

At the other extreme, some individual impacts were observed to produce more than 1000 sputtered atoms. Thus, these individual “mega-events” contribute disproportionately to the average sputtering yields. Fig. 2a–c provide information about the sputtering statistics for individual monomer, dimer, and trimer impacts at 100 keV/ incident atom bombarding energy. Yields per individual impact are plotted on the horizontal axis. On the vertical axis the yields per individual impact are multiplied by the number of impacts with

Table 1
Sputtering statistics – impacts producing zero sputtered atoms

	Monomers	Dimers	Trimers
100 keV/atom	198	111	44
0.10 reflection coefficients	(39.6%)	(22.2%)	(8.8%)
200 keV/atom	190	152	109
0.10 reflection coefficients	(38.0%)	(30.4%)	(19.8%)
200 keV/atom	191	153	99
0.15 reflection coefficients	(38.2%)	(30.6%)	(19.8%)

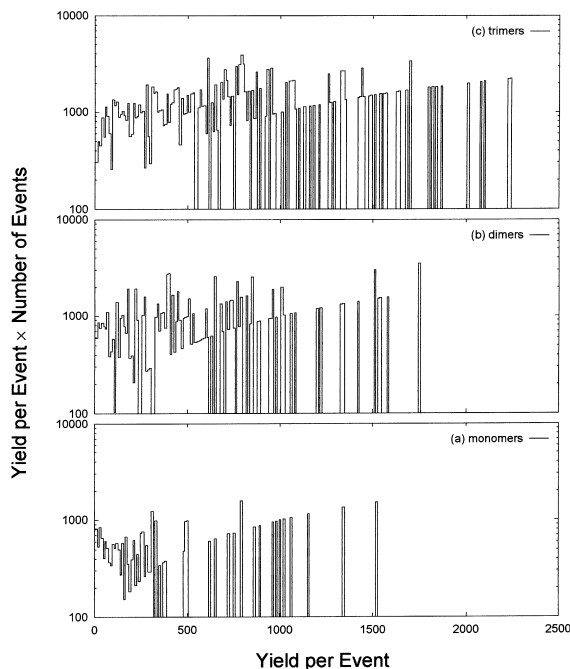


Fig. 2. Contributions to the total sputtering yield from events of different size computed with 100 keV/atom (a) monomer, (b) dimer and (c) trimer projectiles. The size of the event (number of sputtered atoms per impact) is plotted on the horizontal axis, while the total yield attributed to events of a given size is plotted on the vertical axis. Similar results were obtained with 200 keV/atom projectiles.

corresponding yields. Very similar results were obtained for the 200 keV/incident atom bombarding energy (with reflection coefficients of 0.10 for both the incident atoms and target atoms). This figure shows that individual events with very large yields (>500 atoms per impact) contribute significantly to the average sputtering yield, and that the largest events remove as much as 15% of the target material.

3.3. Sputtering yields

The average sputtering yields obtained from the 100 and 200 keV/atom simulations that used the 3000 fs cutoff time and reflection coefficients of 0.10 and 0.15 for incident and target atoms are summarized in Table 2. The total dimer and trimer yields exhibit significant nonlinearities – up to 47% for dimers, and up to 92% for trimers. (The yield

nonlinearity for clusters is defined as $(Y_n/n - Y_1)/Y_1 \times 100\%$.) While these are substantial nonlinearities they are not as large as the nonlinearities observed experimentally, which range up to $\sim 400\%$ for trimer bombardment at these energies.

In Table 2 information about sputtering yields also is presented for individual impacts that produced both fewer and more than the average sputtering yield. Individual impacts that produce fewer than the average sputtering yield contribute between 10% and 18% to the total yield for a given case. This is not surprising considering the relatively large number of impacts that produce no sputtered atoms, and considering the contribution of mega-events to the total yield.

We find that dimer and trimer impacts that produce fewer than the average yield of sputtered atoms show greater nonlinearities than the dimer and trimer impacts that produce more than the average number of sputtered atoms. The nonlinearities ranged from 72% to 93% for dimer impacts producing fewer than the average number of sputtered atoms, while they ranged from 33% to 42% for dimer impacts producing more than the average number of sputtered atoms. For trimer impacts producing less than the average number of sputtered atom, the nonlinearities ranged from 140% to 166%. While for trimer impacts producing more than the average number of sputtered atoms, the nonlinearities ranged from 29% to 84%.

We believe that these differences can be traced to limitations in the size of the targets used for the simulations, and in the reflection algorithm. These points are discussed in greater detail below.

3.4. Temporal development of collision cascades

Distributions of the number of ejected atoms per incident ion as a function of the time of ejection for the 100 keV/atom simulations with the bond-weakening algorithm turned on are shown in Fig. 3 for monomer, dimer, and trimer impacts. The dimer and trimer results have been normalized to show yields per incident atom. Turning off the bond-weakening algorithm had little effect on the yields or temporal distribution of ejected atoms, as can be seen in Fig. 4. Similar normalized yields vs.

Table 2

	Monomers	Dimers	Trimers
<i>Part (a) Sputtering yields – total</i>			
100 keV/atom – 0.10 reflection coefficients	69.9	201.0	369.0
Nonlinearity		44%	59%
200 keV/atom – 0.10 reflection coefficients	35.4	104.2	204.3
Nonlinearity		47%	92%
200 keV/atom – 0.15 reflection coefficients	54.3	149.2	226.3
Nonlinearity		37%	39%
<i>Part (b) Sputtering yields – “below average” events</i>			
100 keV/atom – 0.10 reflection coefficients	8.7	30.0	68.8
Nonlinearity		72%	164%
200 keV/atom – 0.10 reflection coefficients	3.8	14.7	30.3
Nonlinearity		93%	166%
200 keV/atom – 0.15 reflection coefficients	5.1	18.0	36.7
Nonlinearity		76%	140%
<i>Part (c) Sputtering yields – “above average” events</i>			
100 keV/atom – 0.10 reflection coefficients	61.2	170.9	300.0
Nonlinearity		40%	63%
200 keV/atom – 0.10 reflection coefficients	31.6	89.5	174.0
Nonlinearity		42%	84%
200 keV/atom – 0.15 reflection coefficients	49.2	131.2	189.7
Nonlinearity		33%	29%

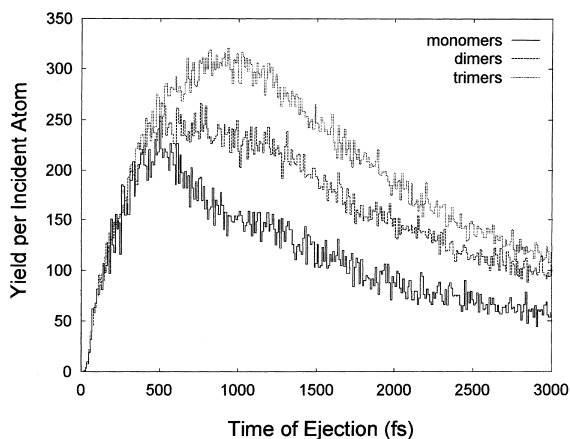


Fig. 3. Normalized sputtering yields vs. ejection time spectra computed for 100 keV/atom monomer, dimer and trimer projectiles. The bond-weakening algorithm was turned on for these calculations. Similar results were obtained with 200 keV/atom projectiles without bond weakening.

ejection time distributions were seen in the 200 keV/atom simulations with a 0.10 reflection coefficient.

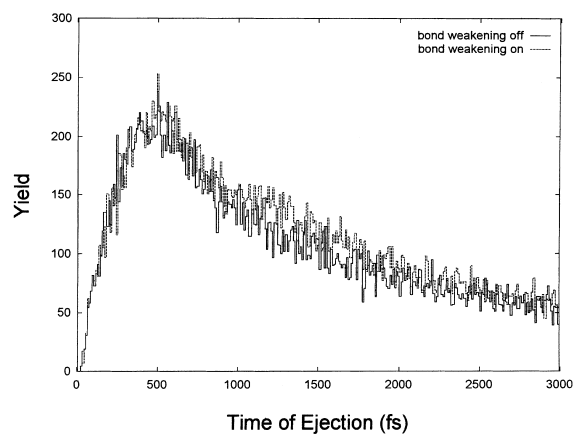


Fig. 4. Comparison of sputtering yields vs. ejection time spectra for 100 keV Au_1 projectiles computed with and without bond-weakening.

Both the 100 and 200 keV/atom distributions for monomer, dimer, and trimer bombardment show that the collision cascades are essentially linear for approximately the first 500 fs after impact. Then substantial nonlinearities develop in the

dimer-and trimer-induced collision cascades. Even though the rate of sputtering decreases after the ballistic phase of the collision cascade (~ 1000 fs), the rate of sputtering remains high for all three cases at the cutoff time of 3000 fs. This is an indication that a substantial amount of material is ejected from the target during the thermal spike phase. It is likely that for many collision cascades the thermal spike phase extends well beyond the 3000 fs cutoff time used in these simulations, and that a substantial part of the experimental yield comes from the thermal spike component.

The effects of sputtering statistics on the development of the thermal spike component have been investigated by making cuts in the data based on the yields per individual impact. For example, in Fig. 5a–b distributions of yields per incident atom vs. ejection time have been plotted separately for individual events with yields less than the average and for events with yields greater than the average. (For dimer and trimer impacts the cuts were made at twice and three times the monomer average, respectively.) The distributions plotted in Fig. 5a show that the events with less than average yield that are initiated by monomers do not produce a significant number of thermal spikes. However, the distributions in Fig. 5a show that for some dimer and trimer impacts with below average yields significant sputtering extends out to the 3000 fs cutoff. This suggests that thermal spike behavior is enhanced by the overlapping collision cascades associated with dimer and trimer impacts.

Events with above average yield produced large numbers of thermal spikes, and exhibited significant nonlinearity. Although, as we have noted in Section 3.3 the degree of nonlinearity is not as large as for the events with less than average yield.

Cuts were also made at yields of 500 for monomer impacts, 1000 for dimer impacts, and 1500 for trimer impacts. For impacts with yields greater than these values, the nonlinearities were quite small. This may be an artifact of the limited target size and the inherent linearity of the reflection algorithm. This “saturation” effect, which can be seen in Fig. 6, also may explain why the yields and nonlinear effects seen in our simulations are not as large as the experimental observations.

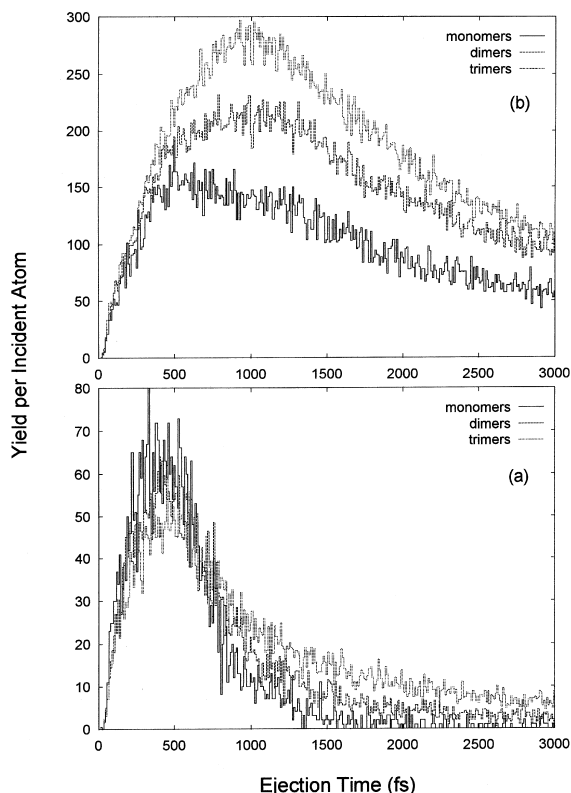


Fig. 5. (a) Normalized sputtering yields vs. ejection time spectra from 100 keV/atom monomer, dimer and trimer impacts that produced below average yields. (b) Similar spectra for impacts that produced above average yields. Similar results were obtained with 200 keV/atom projectiles.

3.5. Energy and angle distributions of sputtered atoms

Normalized energy distributions of sputtered atoms from the 100 keV/atom simulations for events with individual yields up to the average yield are shown in Fig. 7a. Similar normalized distributions for events with individual yields above the average yield are shown in Fig. 7b. For impacts producing below average yields, nonlinear effects are most pronounced for ejected atoms with the lowest energies (≤ 2.5 eV). Because of their very low energies these atoms are likely to have been sputtered during the thermal spike phase of the collision cascade. At the very lowest energies the nonlinearity approaches 400% for trimers,

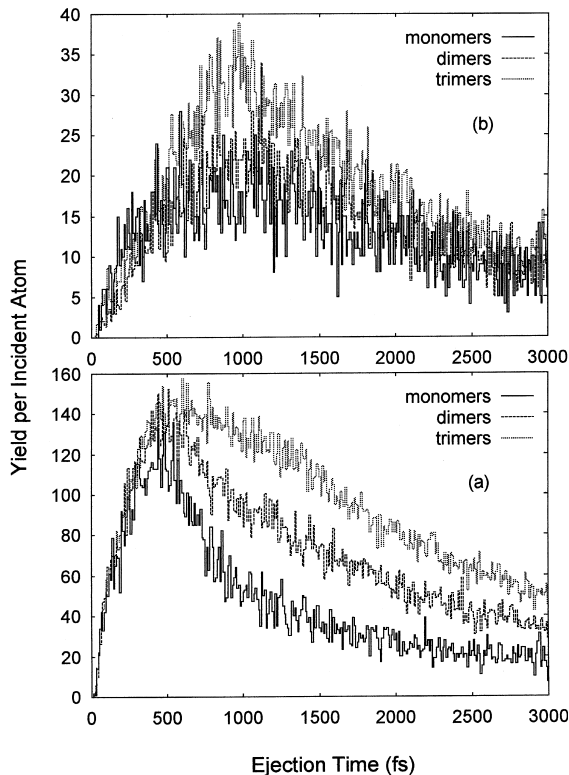


Fig. 6. (a) Normalized sputtering yields vs. ejection time spectra from 100 keV/atom monomer, dimer and trimer impacts that produced total yields below 500, 1000 and 1500, respectively. (b) Similar spectra for impacts that produced total yields greater than 500, 1000 and 1500, respectively.

which is close to the experimentally observed value. In comparison, for impacts producing above average yields, the nonlinearities are nearly constant even for relatively energetic sputtered atoms and do not exceed $\sim 100\%$. The contributions to the energy spectra at the lowest energies are large, but the spectra do not rise as rapidly as for the impacts producing less than average yields. This may be an indication of “saturation” during the thermal spike phase for the largest sputtering events. Similar results were seen in the simulations with 200 keV/atom projectiles.

There are pronounced differences in the polar angle distributions of sputtered atoms for impacts with yields below the average yield compared to impacts with yields above the average. Normalized

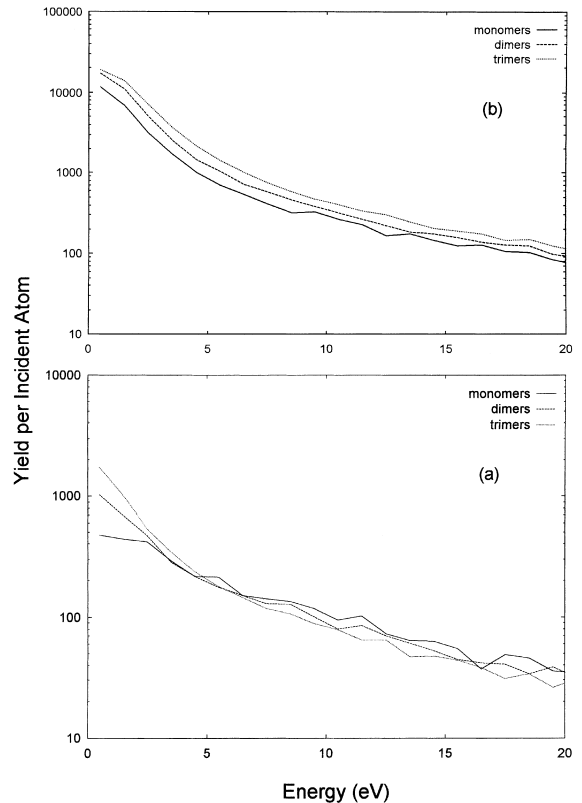


Fig. 7. (a) Normalized energy spectra of sputtered atoms from 100 keV/atom monomer, dimer and trimer impacts that produced above average yields. (b) Similar spectra for impacts that produced below average yields. Similar results were obtained with 200 keV/atom projectiles.

polar angle distributions from the simulations with 100 keV/atom projectiles are shown in Fig. 8a–b. For the impacts with below average yields, the distributions are relatively forward peaked, and the nonlinearity is most pronounced at large ejection angles. The distributions from the impacts with above average yields are much broader, and nonlinear behavior is present at all angles. An unusual feature of all the distributions from impacts with above average yields and the distributions for dimer and trimer impacts with below average yields is the relatively large number of atoms sputtered at large polar angles. This large angle behavior is not seen in ballistic sputtering. However, it is consistent with evaporation from thermal spikes.

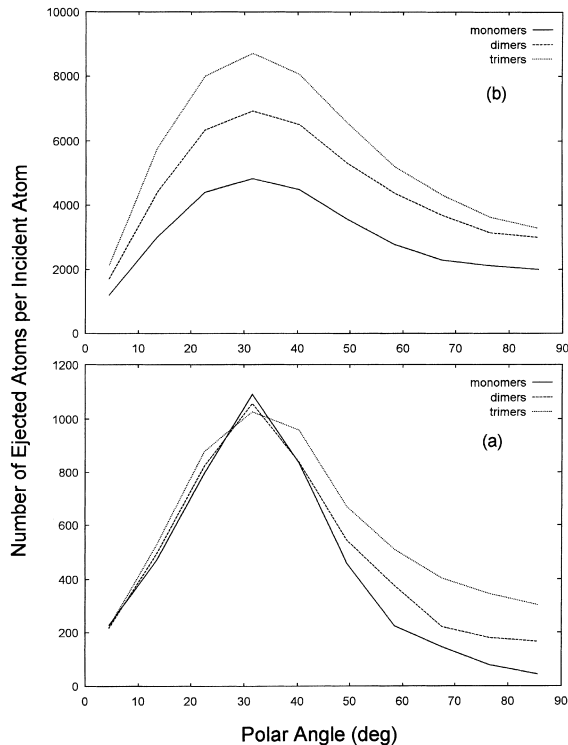


Fig. 8. (a) Polar-angle distributions of sputtered atoms from 100 keV/atom that produced below average yields. (b) Similar spectra from impacts that produced above average yields. All spectra have been normalized to the number of incident atoms, but not to unit solid angle.

4. Discussion

Although our simulation results have been limited by the available computer resources, they suggest that the very large sputtering yields observed in Ref. [1] are the result of substantial nonlinearities during both the collisional and the thermal spike phases of the collision cascades. Our computed energy distributions of sputtered atoms show that very large numbers of atoms are sputtered with very low energies, which is an indication that these processes frequently lower the surface binding energy significantly, which further contributes to large yields. The polar-angle distributions of sputtered atoms are consistent with this observation.

Our simulation results also show that for many cascades the thermal spike phase lasts considerably longer than the 3 ps cutoff time used in our cal-

culations. We have not estimated contributions to the yield from the later stages of the thermal spike because our code did not include an algorithm to provide for target cooling. Nevertheless, it appears that the contribution to the yield from the later stage of the thermal spike could be considerable, and could account for part of the difference between the simulated and experimental yields.

Our simulations also show that at these high bombarding energies the statistics of individual sputtering events plays an important role in the ejection process. We computed yields from individual trimer impacts that ranged up to almost 2500 sputtered atoms (~20% of the total number of atoms in the target). There are two consequences of such a rapid removal of material from the target that may be relevant to the experimental observations and analysis of Ref. [1]. First, this suggests that a substantial fraction of the yield could be in the form of large clusters of atoms. Second, given the wide variation in individual event yields, it probably is not meaningful to discuss an effective initial radius ρ_0 for thermal spikes initiated by such high energy clusters.

The reflection algorithm that was used to simulate the transfer of momentum from the bulk is nonlinear only to the extent that the collision cascade within the actual simulation target is nonlinear. Thus, the algorithm may underestimate the contributions to nonlinear yields that would arise from cascades that become nonlinear at greater depths. This may explain the “saturation” effect that we see for events with the largest yields.

Finally we note that in our simulations all the incident ions and clusters impacted normally on pristine targets. In the experiments work the target surfaces become damaged as the total fluence increases. This could lead to substantial changes in surface topography, such that the effective angle of incidence for incoming ions and clusters differs considerably from 90°. This also could affect the experimental yields.

5. Conclusions

Our simulations show that nonlinearities during both the ballistic and thermal spike phases of the

collision cascade contribute significantly to the very large sputtering yields observed in the bombardment of gold targets with small gold clusters. Additional theoretical work is needed to determine why experimental values of Y/n^2 vs. total cluster energy (Y is the yield per incident atom) fall on an almost universal curve. Likewise, additional experimental work is needed to determine the mass distribution of sputtered material at these bombarding energies.

References

- [1] H.H. Andersen, A. Brunelle, S. Della-Negra, J. Depauw, Y. LeBeyec, Phys. Rev. Lett. 80 (1998) 5433.
- [2] P. Sigmund, Phys. Rev. 184 (1969) 383.
- [3] P. Sigmund, Phys. Rev. 187 (1969) 768.
- [4] P. Sigmund, C. Claussen, J. Appl. Phys. 52 (1981) 990.
- [5] D.E. Harrison Jr., Crit. Rev. Sol. State and Mat. Sci. 14 (1998) S1.
- [6] M.H. Shapiro, T.A. Tombrello, D.E. Harrison Jr., Nucl. Instr. and Meth. B 30 (1988) 152.
- [7] B.J. Garrison, N. Winograd, D.M. Deaven, C.T. Reiman, D.Y. Lo, T.A. Tombrello, D.E. Harrison Jr., M.H. Shapiro, Phys. Rev. B 37 (1988) 7197.
- [8] M.H. Shapiro, T.A. Tombrello, Nucl. Instr. and Meth. B 58 (1991) 161.
- [9] K. Gärtner et al., Nucl. Instr. and Meth. B 102 (1995) 183.
- [10] J. Lindhard, M. Scharff, H.E. Schiott, K. Dan. Vidensk. Selsk. Mat. Fys. Medd. 33 (1963) 14.
- [11] M.H. Shapiro, T.A. Tombrello, Nucl. Instr. and Meth. B 90 (1994) 473.
- [12] D.A. Bromley, in: S.P. Parker (Ed.), McGraw-Hill Encyclopedia of Physics, 2nd ed., McGraw-Hill, New York, 1993, p. 276.